Incorporating Nuclear Quantum Effects in Molecular Dynamics with Constrained Minimized Energy Surface

Zehua Chen and Yang Yang*

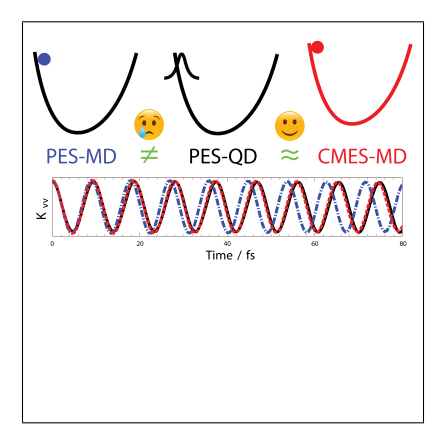
Theoretical Chemistry Institute and Department of Chemistry, University of Wisconsin-Madison, 1101 University Avenue, Madison, WI 53706, USA

E-mail: yyang222@wisc.edu

Abstract

The accurate incorporation of nuclear quantum effects in large-scale molecular dynamics simulations remains a significant challenge. Recently, we combined constrained nuclear-electronic orbital (CNEO) theory with classical molecular dynamics (MD) and obtained a new approach (CNEO-MD) that can accurately and efficiently incorporate nuclear quantum effects in classical simulations. In this Letter, we provide the theoretical foundation for CNEO-MD by developing an alternative formulation of the equations of motion for molecular dynamics. In this new formulation, the expectation values of quantum nuclear coordinates evolve classically on an effective energy surface that is obtained from a constrained energy minimization procedure when solving for the quantum nuclear wave function, thus enabling the incorporation of nuclear quantum effects in classical molecular dynamics simulations. For comparison with other existing approaches, we examined a series of model systems and found that this new MD approach is significantly more accurate than the conventional way of performing classical molecular dynamics, and it also generally outperforms centroid molecular dynamics and ring-polymer molecular dynamics in describing vibrations in these model systems.

TOC Graphic



Keywords

 ${\it nuclear quantum effects, molecular dynamics, multicomponent quantum theory, vibrational spectra$

Nuclear quantum effects (NQEs)¹ have a great impact on the structural, thermodynamical, and kinetic properties of a wide range of chemical and biological systems.² They usually include zero-point and tunneling effects and are significant when light nuclei, such as hydrogen, are present. The accurate incorporation of NQEs in molecular simulations is important for understanding many fundamental properties but remains a significant challenge for large-scale molecular simulations. For example, the anomalous properties of water are closely related to the NQEs of the complex hydrogen bond network^{3,4} and thus cannot be fully explained with conventional classical molecular dynamics (MD) without an accurate inclusion of NQEs.⁵

There have been many theoretical developments on the incorporation of NQEs in molecular simulations. Quantum wave packet dynamics is based on the exact time evolution of a quantum system according to the time-dependent Schrödinger equation and can give theoretical predictions that accurately match to experiments. ^{6–10} Quantum trajectory methods ¹¹ are based on the de Broglie-Bohm formulation of quantum mechanics, ^{12–17} which attributes quantum effects to the quantum potential, and with a reasonable approximation to the quantum potential, quantum trajectory methods have been applied to many model systems and give accurate results. ^{18,19} Multicomponent quantum theories ^{20–26} also include NQEs by simultaneously treating both electrons and key nuclei quantum mechanically, which do not rely on conventional Born-Oppenheimer potential energy surfaces (PESs). Their real-time dynamics simulations. ^{27–31} can be performed through the quantum time evolution of multicomponent wave functions or density matrices, which have been used to study practical chemical problems, such as proton transfer processes. ³²

Although the aforementioned methods are highly accurate in describing NQEs, they are often hindered by their high computational costs in large molecular or bulk systems. This challenge has been partially addressed using methods based on classical simulations. Some empirical force fields ³³ have been used to include NQEs implicitly and have been able to treat hydrogens and deuteriums differently in water. ³⁴ Generalized Langevin Equation thermostat

with optimized parameters is also able to include NQEs and has been applied to obtain several static properties. 35,36 The semi-classical initial value representation (SC-IVR) 37 and its approximate variants ^{38,39} are also able to produce accurate correlation functions with classical simulations. Methods based on the path integral formulation of quantum mechanics 40,41 are most popular for the inclusion of NQEs. By simultaneously simulating a set of coupled replicas for a system, path integral molecular dynamics (PIMD) 42,43 is able to capture NQEs and accurately describe static properties of the system. 44 Its extensions such as centroid molecular dynamics (CMD)^{45,46} and ring-polymer molecular dynamics (RPMD)⁴⁷ can describe dynamical properties using approximate correlation functions. However, while dynamical properties from CMD and RPMD are considerably more accurate than those from conventional MD, challenges still exist with the curvature problem in CMD and spurious frequencies in RPMD. Both of these problems can lead to unreliable vibrational spectra, ⁴⁸ although several recent developments can mitigate them to some extent, including thermostatted RPMD, ^{49,50} Matsubara dynamics, ⁵¹ and quasicentroid molecular dynamics. ^{52,53} Furthermore, in contrast with PIMD, which has many techniques developed to make it as efficient as conventional MD, 54-57 currently there are only a limited number of techniques available⁵⁸ to accelerate RPMD/CMD simulations other than massive parallelization, and thus, the efficient simulation of dynamical properties remains a challenge.

In this Letter, we present an alternative formulation of the equations of motion for classical molecular simulations, with which NQEs can be described using an effective PES that is in practice approximated by a constrained minimized energy surface (CMES). This formulation serves as the theoretical foundation for our recently developed MD approach based on constrained nuclear-electronic orbital theory (CNEO-MD). For comparison with existing approaches, we examine a series of model systems. We first show that CMES-MD remains exact for the harmonic oscillator model. Then, with a Morse oscillator model and a quartic double-well potential model, we show that CMES-MD is generally much more accurate in describing vibrations and tunneling effects than the conventional way of performing classical

MD and is comparable to or slightly better than CMD and RPMD.

We start with the polar representation of a time-dependent wave function $\psi(\boldsymbol{x},t) = A(\boldsymbol{x},t) \exp(\mathrm{i}S(\boldsymbol{x},t)/\hbar)$, where the amplitude part A and the phase part S are both real. For simplicity, we assume in our derivation that there is only one quantum particle, but this formulation can be easily generalized to multiple quantum particle cases if the particles can be assumed to be distinguishable, such as nuclei in regular molecular and bulk systems. Additionally, we will assume that no magnetic field is present, although we note that magnetic fields can be important in some occasions and the corresponding formulation can be explored in the future. With the polar representation, the kinetic energy can be decomposed into two terms

$$\langle \hat{T} \rangle (t) = \int d\mathbf{x} A(\mathbf{x}, t) \frac{(-i\hbar \nabla)^2}{2m} A(\mathbf{x}, t) + \frac{1}{2m} \int d\mathbf{x} A^2(\mathbf{x}, t) [\nabla S(\mathbf{x}, t)]^2.$$
(1)

The first term is the kinetic energy evaluated with the amplitude function A only. Since A is associated with the real space probability density distribution with $\rho(\boldsymbol{x},t) = A^2(\boldsymbol{x},t)$, this term can be perceived as the kinetic energy due to quantum delocalization, or the zero-point kinetic energy. In the second term, the key quantity ∇S is associated with the observable momentum and is related to the momentum field in Bohmian mechanics $^{12-17}$ with the definition $\boldsymbol{p}(\boldsymbol{x},t) = \nabla S(\boldsymbol{x},t)$. Since $A^2(\boldsymbol{x},t)$ is the probability density, this term can be viewed as the kinetic energy associated with the observable momentum \boldsymbol{p} .

We define the variance of the observable momentum as the variance of the momentum field:

$$\sigma_{\mathbf{p}}^{2}(t) \equiv \int d\mathbf{x} A^{2}(\mathbf{x}, t) [\nabla S(\mathbf{x}, t)]^{2} - \langle \hat{\mathbf{p}} \rangle^{2}(t), \qquad (2)$$

then the kinetic energy can be further expressed as

$$\langle \hat{T} \rangle(t) = \langle A(t) | \hat{T} | A(t) \rangle + \frac{\langle \hat{\mathbf{p}} \rangle^2(t)}{2m} + \frac{\sigma_{\mathbf{p}}^2(t)}{2m}.$$
 (3)

The terms in Eq. 3 correspond to, respectively, the zero-point kinetic energy, the classical kinetic energy associated with the expectation value of the observable momentum, and an energy contribution from the variance of the observable momentum field.

Another way of expressing the kinetic energy is simply $\langle \hat{T} \rangle(t) = \langle \hat{H} \rangle(t) - \langle \hat{V} \rangle(t)$, which can be plugged into the left side of Eq. 3. Then by taking the time derivative on both sides of the equation, it can be simplified into

$$\frac{\langle \hat{\boldsymbol{p}} \rangle}{m} \cdot \frac{\mathrm{d} \langle \hat{\boldsymbol{p}} \rangle}{\mathrm{d}t} = \left\langle \frac{\partial V}{\partial t} \right\rangle - \frac{\mathrm{d}}{\mathrm{d}t} \langle A(t) | \hat{H}(t) | A(t) \rangle - \frac{\mathrm{d}}{\mathrm{d}t} \frac{\sigma_{\boldsymbol{p}}^2}{2m}. \tag{4}$$

Note that we have used the relationship $d\langle \hat{H}\rangle(t)/dt = \langle \partial V/\partial t \rangle$ in the derivation. Eq. 4 relates the time dependence of momentum to the time dependence of energetic terms. While Eq. 4 is exact, in order to make it into an equation of motion that can be practically used in MD simulations, we next proceed with an approximation that builds a connection between quantum states and the classical phase space.

Conventionally, when assuming the potential is slowly varying in space, the Ehrenfest theorem provides a connection between the classical Newtonian dynamics in the phase space (X, P) and the evolution of quantum expectation position and momentum $(\langle \hat{x} \rangle, \langle \hat{p} \rangle)$. Here we build on the same mapping philosophy but instead of assuming the behavior of the potential, we approximate the quantum state as the energy-minimized state for a given phase space point. That is, when the system is at a particular phase space point given by an expectation position and an expectation momentum, i.e., $(\langle \hat{x} \rangle, \langle \hat{p} \rangle) = (X, P)$, the quantum state $|\psi\rangle$ always adapts to the energy-minimized state for that phase space point. We note that this approximation is an adiabatic approximation and is not trivially justifiable, however, to keep the flow of the derivation, we leave discussions of its applicability as well as limitations for the later part of this Letter.

Under this adiabatic approximation, the quantum state $|\psi\rangle$ becomes an explicit function of (X, P) and an implicit function of time t, i.e., $|\psi\rangle(X(t), P(t))$. At a particular phase

space point (X(t), P(t)) that the system evolves to at time t, the state can be obtained with a constrained energy minimization procedure. The corresponding Lagrangian is

$$\mathcal{L} = \langle \psi | \hat{H}(t) | \psi \rangle + \boldsymbol{f} \cdot (\langle \psi | \hat{\boldsymbol{x}} | \psi \rangle - \boldsymbol{X}(t))$$
$$- \boldsymbol{v} \cdot (\langle \psi | \hat{\boldsymbol{p}} | \psi \rangle - \boldsymbol{P}(t)) - \tilde{E}(\langle \psi | \psi \rangle - 1), \tag{5}$$

where f is the Lagrange multiplier associated with the expectation position, v is the Lagrange multiplier associated with the expectation momentum, and \tilde{E} is the Lagrange multiplier associated with the wave function normalization. This Lagrangian can be further expressed in terms of A and S by

$$\mathcal{L} = \langle A|\hat{H}(t)|A\rangle + \frac{1}{2m} \int d\boldsymbol{x} A^{2} (\nabla S)^{2}$$

$$+ \boldsymbol{f} \cdot (\langle A|\hat{\boldsymbol{x}}|A\rangle - \boldsymbol{X}(t)) - \boldsymbol{v} \cdot \left(\int d\boldsymbol{x} A^{2} \nabla S - \boldsymbol{P}(t) \right)$$

$$- \tilde{E}(\langle A|A\rangle - 1).$$
(6)

Making the Lagrangian function stationary with respect to the variation of ∇S and A leads to $A^2(\nabla S/m - \mathbf{v}) = 0$ and

$$\left[\hat{H}(t) + \frac{(\nabla S)^2}{2m} + \boldsymbol{f} \cdot \hat{\boldsymbol{x}} - \boldsymbol{v} \cdot \nabla S\right] |A\rangle = \tilde{E}|A\rangle.$$
 (7)

Further combining these equations with the expectation position constraint, the expectation momentum constraint, and the normalization constraint gives $\mathbf{v} = \mathbf{P}(t)/m$, $\nabla S(\mathbf{x}) = m\mathbf{v} = \mathbf{P}(t)$, then the eigenvalue equation can be simplified to

$$[\hat{H}(t) + \boldsymbol{f} \cdot \hat{\boldsymbol{x}}]|A\rangle = \left(\tilde{E} + \frac{\boldsymbol{P}^2}{2m}\right)|A\rangle.$$
 (8)

The eigenvalue $\tilde{E}+\mathbf{P}^2/2m$, eigenstate $|A\rangle$, and the Lagrange multiplier \mathbf{f} can be solved under the expectation position and normalization constraints for $|A\rangle$. Note that interestingly, the

solution of the amplitude function A only depends on the expectation position constraint, and the expectation momentum constraint only affects the phase function S.

The fact that the constrained minimization requires ∇S to agree with the expectation momentum $(\nabla S(\boldsymbol{x}) = \boldsymbol{P}(t))$ naturally leads to $\sigma_{\boldsymbol{p}}^2 = 0$ according to the definition in Eq. 2, and with the quantum state $|A\rangle$ obtained as an explicit function of \boldsymbol{X} and thus an implicit function of t, we can simplify Eq. 4 into

$$\frac{\langle \hat{\boldsymbol{p}} \rangle}{m} \cdot \frac{\mathrm{d} \langle \hat{\boldsymbol{p}} \rangle}{\mathrm{d}t} \approx -\left\langle \frac{\mathrm{d}A}{\mathrm{d}t} \middle| \hat{H}(t) \middle| A \right\rangle - \left\langle A \middle| \hat{H}(t) \middle| \frac{\mathrm{d}A}{\mathrm{d}t} \right\rangle$$

$$= -\frac{\mathrm{d}\boldsymbol{X}}{\mathrm{d}t} \cdot \left[\langle \nabla_{\boldsymbol{X}} A \middle| \hat{H}(t) \middle| A \rangle \right]$$
(9)

$$+ \langle A|\hat{H}(t)|\nabla_{\mathbf{X}}A\rangle \Big] \tag{10}$$

$$= -\frac{\langle \hat{\boldsymbol{p}} \rangle}{m} \cdot \nabla_{\boldsymbol{X}} \langle A | \hat{H}(t) | A \rangle. \tag{11}$$

Note that here we have used $d\mathbf{X}/dt = d\langle \hat{\mathbf{x}} \rangle/dt = \langle \hat{\mathbf{p}} \rangle/m$. According to classical mechanics, it is natural to assume that the change of $\langle \hat{\mathbf{p}} \rangle$ should have an opposite direction to the energy gradient term $(\nabla_{\mathbf{X}} \langle A|\hat{H}(t)|A\rangle)$, therefore, the common prefactor $|\langle \hat{\mathbf{p}} \rangle|/m$ can be dropped, and we arrive at the final expression

$$\frac{\mathrm{d}\langle \hat{\boldsymbol{p}}\rangle}{\mathrm{d}t} \approx -\nabla_{\boldsymbol{X}}\langle A|\hat{H}(t)|A\rangle \equiv -\nabla_{\boldsymbol{X}}V^{\mathrm{CMES}}(\boldsymbol{X}), \tag{12}$$

where V^{CMES} is the constrained minimized energy surface associated with the amplitude part $|A\rangle$. It can also be viewed as an effective potential energy surface that includes not only the potential energy but also the quantum delocalization kinetic energy. Eq. 12, together with $\mathrm{d}\langle\hat{x}\rangle/\mathrm{d}t=\langle\hat{p}\rangle/m$, forms the equations of motion for CMES-MD. These equations of motion present an alternative way of performing MD simulations but with NQEs incorporated. They are highly similar in structure to Newton's equations used in conventional MD simulations, with the difference that the time evolution is now on the quantum expectation positions and momenta rather than the classical ones.

We note that there have been prior works⁵⁹⁻⁶¹ that arrived at the same equations of motion within the framework of Feynman's path-integral formulation of quantum mechanics. Within the path-integral framework, the effective potential guides the motion of the ring-polymer centroid, and is claimed to be equal to the zero-temperature limit of the centroid potential for CMD. Therefore it has been used to gain insight into the behavior of CMD. In our work presented here, with a formal derivation from the conventional formulation of quantum mechanics, these equations provide a new way of performing classical molecular simulations with the effective potential utilized to guide the classical motion of the quantum expectation values.

Additionally, we note that this formulation serves as the theoretical foundation for our recently published work of CNEO-MD, ⁶² in which constrained nuclear electronic orbital density functional theory (CNEO-DFT) ^{63–65} is employed to obtain CMESs for practical molecular systems and used for MD simulations. CNEO-MD is a generalization of CMES-MD when the electronic part is also explicitly considered in the energy minimization procedure. More detailed derivation on their connections can be found in Section S3 of the Supporting Information. With a series of gas phase molecules, we have demonstrated the excellent agreement between the CNEO-MD vibrational spectra and the experimental spectra. ⁶² Specifically for highly anharmonic O–H and C–H stretching modes, CNEO-MD significantly outperforms conventional DFT-based *ab initio* molecular dynamics, with errors in peak positions reduced by one order of magnitude, but at essentially the same computational cost.

For comparison with other existing approaches, herein, we investigate the model systems of a harmonic oscillator, a Morse oscillator and a quartic double-well potential. These model systems are chosen because they have easily accessible exact quantum solutions, avoid errors associated with real systems such as electron correlations, and are affordable for CMD and RPMD simulations. For these model systems, we scan a set of discrete f values in Eq. 8 to solve for the CMESs. Specifically, for each f, the constrained eigenvalue equation is solved numerically on a grid and the energy as a function of the corresponding nuclear

expectation position is obtained. Afterwards, the energies as well as the gradients at arbitrary expectation positions are obtained by cubic spline interpolation during the dynamics simulations. We note that for multi-dimensional models and practical chemical systems, this way of constructing CMES becomes computationally expensive. Fortunately, in practical systems, CNEO-DFT^{63,64} minimizes the total energy of a system with nuclear expectation position constraints and therefore can be used to calculate the CMES on the fly. This current work will focus more on building the theoretical foundation and exploring the strengths and limitations of CMES-MD with the help of the simple models.

In our practical model calculations, classical MD and CMES-MD are performed with an in-house python script. Note that throughout the Letter, by conventional MD or classical MD we mean classical molecular simulations based on a Boltzmann sampling of the initial velocity according to the designated temperature and evolving with classical Newtonian equations. We are aware that there exist other methods such as quasi-classical MD 66 and SC-IVR^{37–39} that are able to include zero-point effects in classical simulations, but they are not referred to as classical MD or conventional MD in this Letter. The total simulation time of all conventional MD and CMES-MD simulations is chosen to be 50 ps, and the trajectories are integrated using the velocity-Verlet algorithm with a time step of 0.5 fs. RPMD and CMD simulations on these one-dimensional models are performed with a modified i-PI package. ⁶⁷ Specifically, a 30 ps PIMD trajectory with 0.1 fs time step is first calculated and used to generate initial configurations for RPMD and CMD. Then RPMD and CMD are performed with a simulation length of 10 ps. For RPMD, the time step is set to 0.1 fs, and for CMD, the time step is 0.003125 fs, and the data are recorded every 0.1 fs. For the Morse oscillator model, RPMD and CMD both use 64 beads in simulations with $T = 50 \,\mathrm{K}$, 32 beads in simulations with $T = 300 \,\mathrm{K}$, and 16 beads in simulations with $T = 1500 \,\mathrm{K}$. For the double-well potential model, the corresponding bead numbers are 128 for $T=50\,\mathrm{K},\,64$ for $T=100\,\mathrm{K},\,$ and 32 for $T = 1500 \,\mathrm{K}$. We perform 1000 NVE simulations whose initial configurations satisfy the Maxwell-Boltzmann distribution to obtain an NVT ensemble average for classical MD and CMES-MD, however, this number is reduced to 50 for RPMD and 30 for CMD to limit the computational cost. After the simulations, the trajectories are used to generate correlation functions. In data processing, a correlation depth of 4096 points is used for MD and CMES-MD. For RPMD and CMD, a larger depth of 16384 points is used because of the shorter time step used. Power spectra are obtained via Fourier transforms of the corresponding velocity autocorrelation functions. They are then averaged to get the *NVT* ensemble-averaged power spectra for each method. The intensities of the averaged power spectra are finally adjusted so that they integrate to a number that is proportional to the simulation temperature.

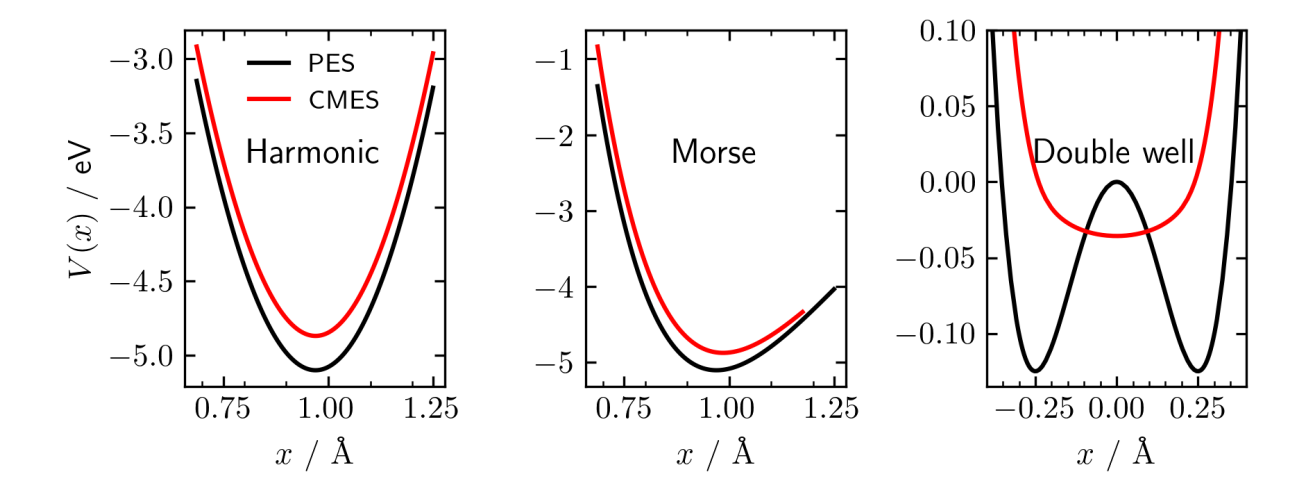


Figure 1: Comparison between the potential energy surface (PES) and constrained minimized energy surface (CMES) for the harmonic oscillator model (left), the Morse oscillator model (middle), and the double-well potential model (right).

The harmonic oscillator $\hat{H} = \hat{p}^2/2m + m\omega^2 (\hat{x} - x_{\rm e})^2/2$ is one particular model for which classical MD gives the same trajectory as the exact quantum theory. CMD and RPMD are also exact for this model system. For CMES-MD, since $\hat{H} + f\hat{x}$ represents the harmonic oscillator with shifted energy and shifted position based on the value of f, the constrained minimized energy state $|A\rangle$ for any expectation position $\langle \hat{x} \rangle = X$ is the ground state wave function of \hat{H} shifted to the expectation position $\langle \hat{x} \rangle = X$. Therefore, the corresponding

energy surface as a function of the expectation position X is

$$V^{\text{CMES}}(X) = \frac{\hbar\omega}{2} + \frac{1}{2}m\omega^2 (X - x_e)^2.$$
 (13)

This effective potential universally shifts the original harmonic potential upwards by $\hbar\omega/2$, which is the zero-point energy for a harmonic oscillator (Fig. 1). This result may seem counterintuitive since conventionally ZPE is considered to be a property of the whole energy surface rather than a point-wise property, however, we note that here the ZPE should be more accurately considered as a quantum delocalization energy, which always exists as the quantum wave packet travels through space. Since classical MD produces the exact trajectory on the harmonic potential, the trajectory produced by CMES-MD on $V^{\rm CMES}$ is also exact without any need for numerical tests.

Compared with the harmonic potential, the Morse potential is a better model for chemical bonds with anharmonic effects. Here we use a Morse potential that can mimic the stretch of the O-H radical and perform simulations using classical MD, CMES-MD, RPMD, and CMD. Fig. 2 shows the velocity autocorrelation functions and the corresponding power spectra of these methods at three different temperatures. The exact quantum results are used as references, which are obtained from the analytical solution of the Morse potential. Compared with the Kubo-transformed quantum velocity autocorrelation function, ⁶⁸ classical MD underestimates the period of the correlation function and therefore severely overestimates the vibrational frequency. RPMD and CMD can more accurately describe the correlation function and their overestimations of the vibrational frequencies are significantly smaller. CMES-MD has the best performance with good agreement with the exact quantum correlation functions and more accurate vibrational frequencies. The good result of CMES-MD at relatively low temperatures are not surprising since CNEO-MD has been known to give accurate vibrational spectra at room temperature, ⁶² and vibrational frequencies obtained from CNEO-DFT Hessian calculations are also in great agreement with experimental val-

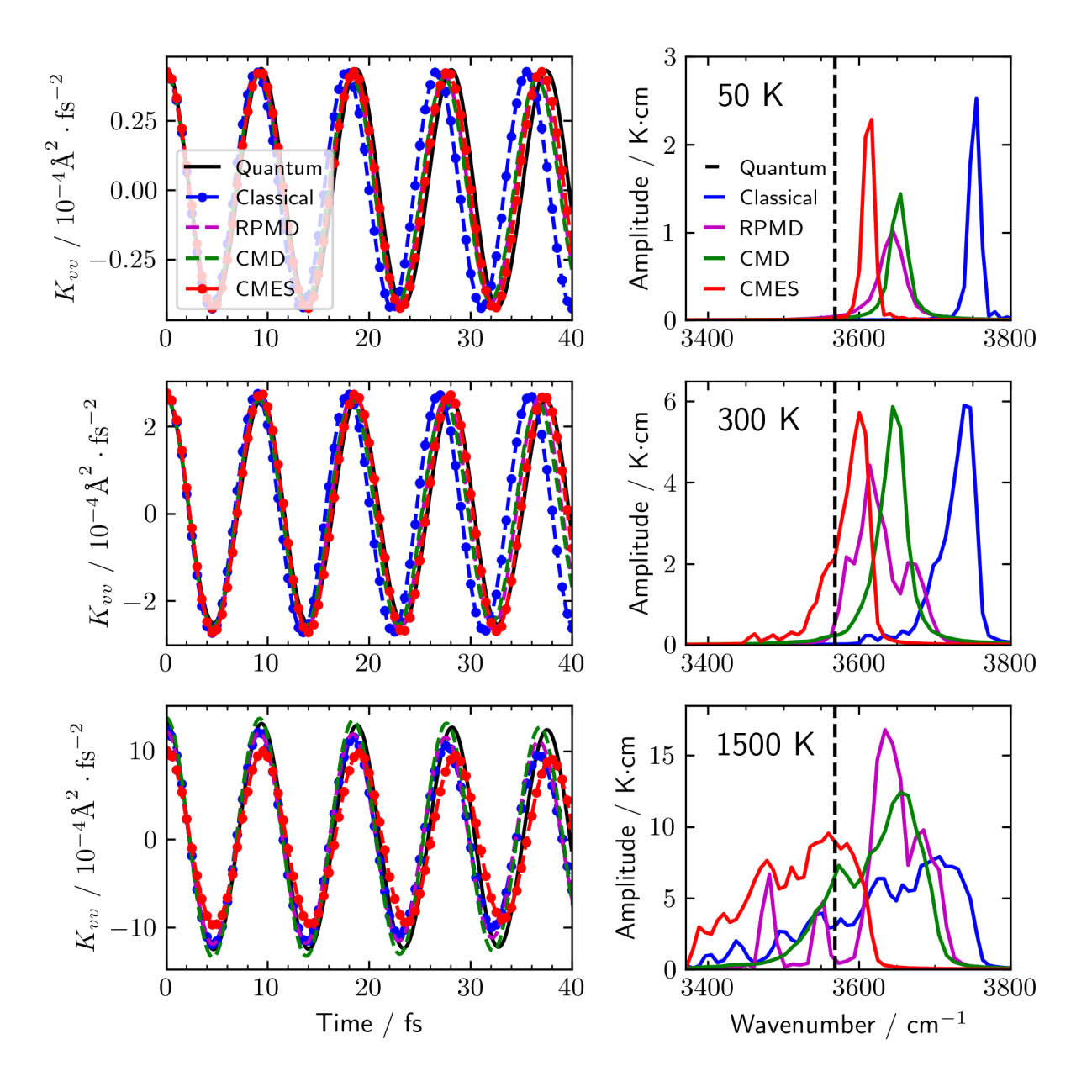


Figure 2: Velocity autocorrelation functions K_{vv} and power spectra of the Morse oscillator mimicking the $^{16}\mathrm{O}^1\mathrm{H}$ radical at 50 K (upper), 300 K (middle) and 1500 K (lower). The potential form is $V(x) = D_\mathrm{e}(\mathrm{e}^{-2\alpha(x-x_\mathrm{e})} - 2\mathrm{e}^{-\alpha(x-x_\mathrm{e})})$, where $D_\mathrm{e} = hc\omega_\mathrm{e}^2/4\omega_\mathrm{e}\chi_\mathrm{e}$ and $\alpha = \sqrt{2\mu hc\omega_\mathrm{e}\chi_\mathrm{e}/\hbar^2}$. All the parameters are the same as those used in Ref. 49, with $\omega_\mathrm{e} = 3737.76\,\mathrm{cm}^{-1}$, $\omega_\mathrm{e}\chi_\mathrm{e} = 84.881\,\mathrm{cm}^{-1}$, and $x_\mathrm{e} = 0.96966\,\mathrm{Å}$. The dashed vertical line represents the exact quantum frequency $3568\,\mathrm{cm}^{-1}$. Two spikes below the quantum frequency in the RPMD $1500\,\mathrm{K}$ spectrum are due to insufficient sampling.

ues, indicating a good zero-temperature limit. 65 As the temperature increases, CMES-MD and other simulation methods start to have broader and red-shifted peaks. For this Morse potential, we observe that CMES-MD produces accurate spectra for a temperature range between 50 K and 1500 K, suggesting the reliability of CMES-MD in the temperature range that most chemical and biophysical reactions are performed at.

Next we investigate a more challenging double-well potential model, in which quantum tunneling is expected to occur. We use a quartic double-well potential with a 0.125 eV barrier height and a 0.5 Å separation between the potential minima, which can roughly represent the potential energy landscape for a practical proton transfer reaction. As shown in Fig. 1, the CMES of this double-well potential is a single well with the minimum located at X=0 due to the symmetrical shape of the ground state wave function with two peaks, whose expectation position is at $\langle \hat{x} \rangle = 0$. As the constrained expectation position deviates from the center, the constrained minimized wave function becomes less symmetrical with more and more excited state characters mixed in, thus increasing the energy and forming a single-well effective potential. Note that this picture has also been observed in previous literature when investigating the zero-temperature limit of CMD. 59,60

On this single-well effective potential, the quantum expectation position moves smoothly between left and right as if the barrier does not exist. This is qualitatively in agreement with the quantum picture, in which the wave function can tunnel back and forth through the barrier with a smooth oscillation for the quantum expectation position. This physical picture can be further quantitatively verified by the agreement between the tunneling frequency by CMES-MD and the exact quantum tunneling frequency (Fig. 3). At low temperatures, classical MD simulations are all trapped in the local minima of the double-well and give position autocorrelation functions that are not vertically centered at zero and a highly overestimated vibrational frequency that is close to the second order derivative at the local minimum, indicating the failure of classical MD in describing tunneling effects. The two path-integral methods show significant differences in the double-well potential model,

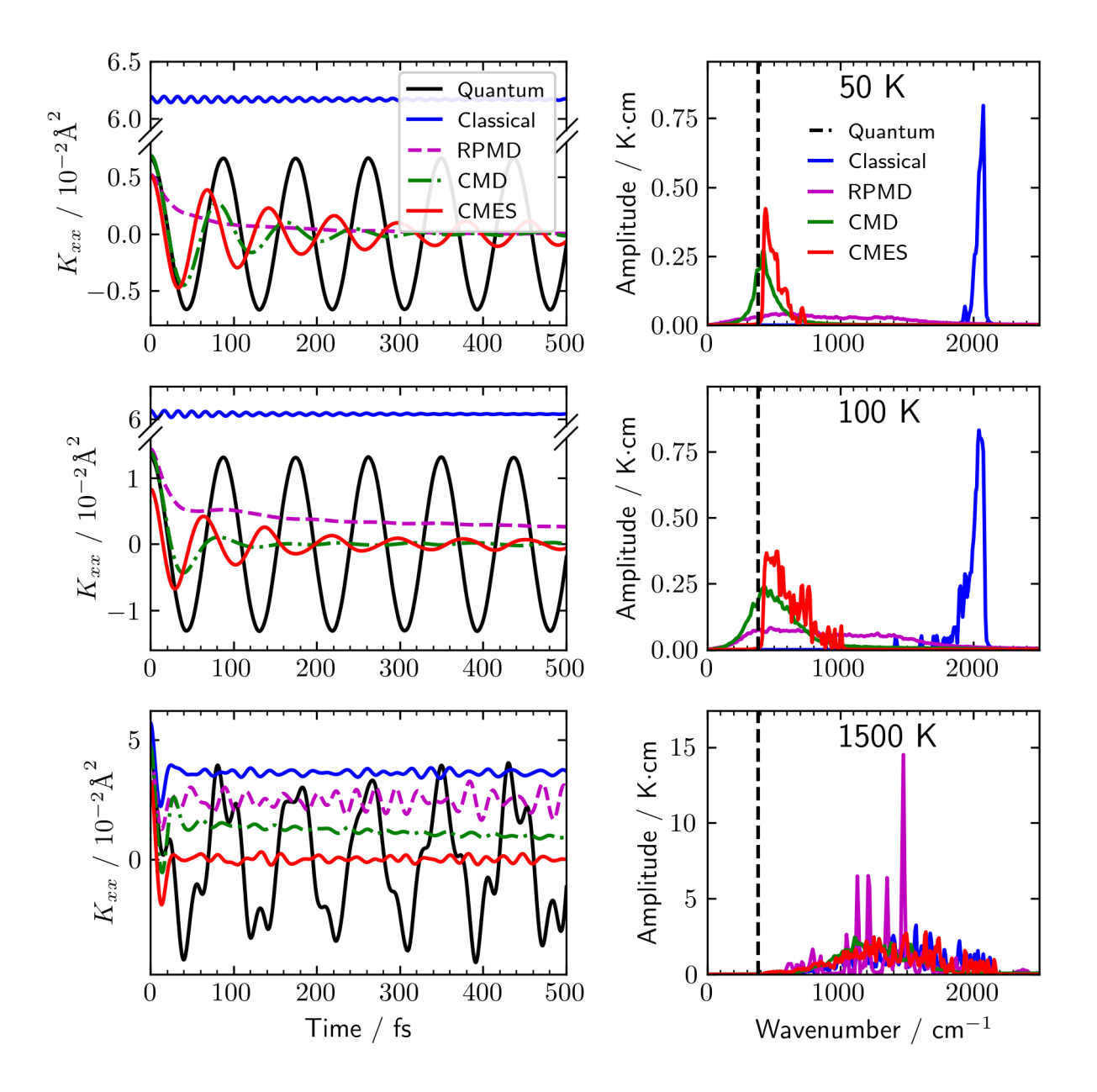


Figure 3: Position autocorrelation function K_{xx} and power spectrum of a proton in the double-well potential at 50 K (upper), 100 K (middle) and 1500 K (lower). The potential form is $V(x) = ax^2 + bx^4$, where $a = -4 \,\mathrm{eV/\mathring{A}}^2$ and $b = 32 \,\mathrm{eV/\mathring{A}}^4$. The dashed vertical line represents the exact quantum frequency $382 \,\mathrm{cm}^{-1}$. Multiple spikes in the RPMD 1500 K spectrum are due to insufficient sampling.

as CMD gives good autocorrelation functions and predicts a relatively sharp peak with an accurate tunneling frequency, whereas RPMD suffers from a fast decay of the correlation function ⁶⁹ and a broad peak that smears over a range of nearly 2000 cm⁻¹. CMES-MD is similar to CMD with a slightly overestimated tunneling frequency. As the temperature increases, classical MD shows redshifts in the peak positions, and CMES-MD and CMD see blueshifts. At 1500 K, all simulation methods behave very similarly with broad peaks that maximize at around 1300-1500 cm⁻¹. All of these results show that CMES-MD performs reasonably well in describing the dynamics in the double-well potential.

We note that quasi-classical MD⁶⁶ can be another way to include zero-point effects in classical simulations and can well describe the vibrational frequency of a Morse potential with an appropriate initial energy. However, there are several known issues related to it. For example, it can lead to zero-point energy leakage, where the excess energy of one high-frequency mode may flow to a low-frequency one, sometimes leading to unphysical molecular dissociations. ^{70,71} Moreover, this method requires the calculation of harmonic frequencies to approximate zero-point energies, which can be problematic if the potential is highly anharmonic. One example is that in the double-well potential, the zero-point energy obtained from the harmonic approximation will be highly inaccurate, and like the classical MD case, the particle may still become trapped in either side of the well if the classical barrier is higher than the zero-point energy. In contrast, CMES-MD and path-integral based methods will not suffer from these problems.

In principle, the effective potential energy surfaces in MD simulations should be temperature-dependent to fully account for nuclear quantum effects. However, although CMES is a temperature-independent effective potential, we observe good performance of CMES-MD over a relatively large temperature range. This suggests that the adiabatic approximation that in essence assumes that the quantum state adapts its wave function to the lowest-energy state for a particular phase space point is reasonable. Nevertheless, it is possible that when the temperature is high and the particle is moving fast, the wave function may not adapt

fast enough to the constrained minimized wave function, thus breaking the adiabatic approximation. Therefore, we expect CMES-MD to be more accurate at low temperatures relative to the mode frequency. Fortunately, for most vibrational modes, the room temperature is still considered low temperature, and therefore CMES-MD can be accurate in a good range of temperatures typically investigated by chemical physicists and biophysicists.

Similarly to conventional MD, the classical treatment brings not only efficiency but also some limitations. For example, quantum coherence is missing, which is reflected by a decreasing amplitude of the correlation function (Fig. 3). Heat capacities will not approach zero when $T \to 0$ K due to the loss of the energy quantization picture. Furthermore, classical dynamics with distinguishable particles is incapable of capturing the exchange effect, which is important in systems with heavily packed particles, such as in a Bose-Einstein condensate. 72,73 Although detailed studies of these possible limitations are beyond the scope of the current work, they are important topics for our future research for better understanding the applicabilities of CMES-MD. We finally note that due to the similarity between CMES-MD and conventional classical MD, in practical systems, we can expect analytical force field models or even machine-learning force fields (ML-FFs)⁷⁴ to be built based on the CMES, which will allow for an even more efficient incorporation of NQEs in MD simulations.

In summary, we provide a new framework for incorporating NQEs in classical molecular simulations. This is achieved through the calculation of the CMES, which serves as the effective potential for classical simulations. In CMES-MD, quantum delocalization and tunneling effects are inherently included and therefore dynamical vibrational frequencies can be accurately described. In simulations of practical systems, CNEO-DFT can be used to obtain the CMES and the resulting CNEO-MD is vastly more computationally efficient than conventional ways of including NQEs based on *ab initio* PESs. It may be further accelerated when combined with modern machine-learning techniques in future developments. As such, CMES/CNEO-MD is a promising new approach to describe NQEs in larger and more complex systems, which will open the door to broader applications.

Acknowledgement

The authors thank David Manolopoulos, Stuart Althorpe, Edwin Sibert, Xi Xu, and James Langford for helpful comments. We are grateful for the funding support from the National Science Foundation under Grant No. 2238473 and from the University of Wisconsin via the Wisconsin Alumni Research Foundation.

Supporting Information Available

Additional details pertaining to the work presented including detailed derivations for the equations of motion of CMES-MD for single-particle and multiple-particle cases, the connection between CNEO-MD and CMES-MD, and a time propagation test on the performance of CMES-MD.

References

- (1) Markland, T. E.; Ceriotti, M. Nuclear Quantum Effects Enter the Mainstream. *Nat Rev Chem* **2018**, *2*, 1–14.
- (2) Pereyaslavets, L.; Kurnikov, I.; Kamath, G.; Butin, O.; Illarionov, A.; Leontyev, I.; Olevanov, M.; Levitt, M.; Kornberg, R. D.; Fain, B. On the Importance of Accounting for Nuclear Quantum Effects in Ab Initio Calibrated Force Fields in Biological Simulations. PNAS 2018, 115, 8878–8882.
- (3) Nilsson, A.; Pettersson, L. G. M. The Structural Origin of Anomalous Properties of Liquid Water. *Nat Commun* **2015**, *6*, 8998.
- (4) Ceriotti, M.; Fang, W.; Kusalik, P. G.; McKenzie, R. H.; Michaelides, A.; Morales, M. A.; Markland, T. E. Nuclear Quantum Effects in Water and Aqueous

- Systems: Experiment, Theory, and Current Challenges. *Chem. Rev.* **2016**, *116*, 7529–7550.
- (5) Zhang, L.; Wang, H.; Car, R.; E, W. Phase Diagram of a Deep Potential Water Model. *Phys. Rev. Lett.* **2021**, *126*, 236001.
- (6) Meyer, H. D.; Manthe, U.; Cederbaum, L. S. The Multi-Configurational Time-Dependent Hartree Approach. *Chemical Physics Letters* **1990**, *165*, 73–78.
- (7) Fleck, J. A.; Morris, J. R.; Feit, M. D. Time-Dependent Propagation of High Energy Laser Beams through the Atmosphere. *Appl. Phys.* **1976**, *10*, 129–160.
- (8) Weichman, M. L.; DeVine, J. A.; Babin, M. C.; Li, J.; Guo, L.; Ma, J.; Guo, H.; Neumark, D. M. Feshbach Resonances in the Exit Channel of the F + CH3OH → HF + CH3O Reaction Observed Using Transition-State Spectroscopy. Nature Chem 2017, 9, 950–955.
- (9) Chen, Z.; Chen, J.; Chen, R.; Xie, T.; Wang, X.; Liu, S.; Wu, G.; Dai, D.; Yang, X.; Zhang, D. H. Reactivity Oscillation in the Heavy–Light–Heavy Cl + CH4 Reaction. Proc. Natl. Acad. Sci. 2020, 117, 9202–9207.
- (10) Chen, W.; Wang, R.; Yuan, D.; Zhao, H.; Luo, C.; Tan, Y.; Li, S.; Zhang, D. H.; Wang, X.; Sun, Z. et al. Quantum Interference between Spin-Orbit Split Partial Waves in the F + HD → HF + D Reaction. Science 2021, 371, 936–940.
- (11) Lopreore, C. L.; Wyatt, R. E. Quantum Wave Packet Dynamics with Trajectories. *Phys. Rev. Lett.* **1999**, *82*, 5190–5193.
- (12) De Broglie, L. Sur la possibilité de relier les phénomenes d'interférence et de diffractiona la théorie des quanta de lumiere. *Comptes Rendus* **1926**, *183*, 447–448.
- (13) De Broglie, L. La structure atomique de la matière et du rayonnement et la Mécanique ondulatoire. CR Acad. Sci. Paris 1927, 184, 273–274.

- (14) Madelung, E. Quantentheorie in hydrodynamischer Form. Z. Physik 1927, 40, 322–326.
- (15) Bohm, D. A Suggested Interpretation of the Quantum Theory in Terms of "Hidden" Variables. I. *Phys. Rev.* **1952**, *85*, 166–179.
- (16) Bohm, D. A Suggested Interpretation of the Quantum Theory in Terms of "Hidden" Variables. II. *Phys. Rev.* **1952**, *85*, 180–193.
- (17) Schleich, W. P.; Greenberger, D. M.; Kobe, D. H.; Scully, M. O. Schrödinger equation revisited. *PNAS* **2013**, *110*, 5374–5379.
- (18) Garashchuk, S.; Rassolov, V. A. Quantum Dynamics with Bohmian Trajectories: Energy Conserving Approximation to the Quantum Potential. *Chemical Physics Letters* **2003**, *376*, 358–363.
- (19) Garashchuk, S.; Rassolov, V. Energy Conserving Approximations to the Quantum Potential: Dynamics with Linearized Quantum Force. J. Chem. Phys. 2004, 120, 1181–1190.
- (20) Thomas, I. L. Protonic Structure of Molecules. I. Ammonia Molecules. *Phys. Rev.* **1969**, 185, 90–94.
- (21) Capitani, J. F.; Nalewajski, R. F.; Parr, R. G. Non-Born-Oppenheimer Density Functional Theory of Molecular Systems. *J. Chem. Phys.* **1982**, *76*, 568–573.
- (22) Tachikawa, M.; Mori, K.; Nakai, H.; Iguchi, K. An Extension of Ab Initio Molecular Orbital Theory to Nuclear Motion. *Chemical Physics Letters* **1998**, *290*, 437–442.
- (23) Kreibich, T.; Gross, E. K. U. Multicomponent Density-Functional Theory for Electrons and Nuclei. *Phys. Rev. Lett.* **2001**, *86*, 2984–2987.
- (24) Webb, S. P.; Iordanov, T.; Hammes-Schiffer, S. Multiconfigurational Nuclear-Electronic Orbital Approach: Incorporation of Nuclear Quantum Effects in Electronic Structure Calculations. J. Chem. Phys. 2002, 117, 4106–4118.

- (25) Ishimoto, T.; Tachikawa, M.; Nagashima, U. Review of Multicomponent Molecular Orbital Method for Direct Treatment of Nuclear Quantum Effect. *Int. J. Quantum Chem.* **2009**, *109*, 2677–2694.
- (26) Pavošević, F.; Culpitt, T.; Hammes-Schiffer, S. Multicomponent Quantum Chemistry: Integrating Electronic and Nuclear Quantum Effects via the Nuclear-Electronic Orbital Method. *Chem. Rev.* **2020**, *120*, 4222–4253.
- (27) Abedi, A.; Maitra, N. T.; Gross, E. K. U. Exact Factorization of the Time-Dependent Electron-Nuclear Wave Function. *Phys. Rev. Lett.* **2010**, *105*, 123002.
- (28) Suzuki, Y.; Abedi, A.; T. Maitra, N.; U. Gross, E. K. Laser-Induced Electron Localization in H₂⁺: Mixed Quantum-Classical Dynamics Based on the Exact Time-Dependent Potential Energy Surface. *Phys. Chem. Chem. Phys.* **2015**, *17*, 29271–29280.
- (29) Zhao, L.; Tao, Z.; Pavošević, F.; Wildman, A.; Hammes-Schiffer, S.; Li, X. Real-Time Time-Dependent Nuclear-Electronic Orbital Approach: Dynamics beyond the Born-Oppenheimer Approximation. J. Phys. Chem. Lett. 2020, 11, 4052–4058.
- (30) Zhao, L.; Wildman, A.; Tao, Z.; Schneider, P.; Hammes-Schiffer, S.; Li, X. Nuclear-Electronic Orbital Ehrenfest Dynamics. *J. Chem. Phys.* **2020**, *153*, 224111.
- (31) Tao, Z.; Yu, Q.; Roy, S.; Hammes-Schiffer, S. Direct Dynamics with Nuclear-Electronic Orbital Density Functional Theory. Acc. Chem. Res. 2021,
- (32) Zhao, L.; Wildman, A.; Pavošević, F.; Tully, J. C.; Hammes-Schiffer, S.; Li, X. Excited State Intramolecular Proton Transfer with Nuclear-Electronic Orbital Ehrenfest Dynamics. J. Phys. Chem. Lett. 2021, 12, 3497–3502.
- (33) Grigera, J. R. An Effective Pair Potential for Heavy Water. J. Chem. Phys. 2001, 114, 8064–8067.

- (34) Ben Abu, N.; Mason, P. E.; Klein, H.; Dubovski, N.; Ben Shoshan-Galeczki, Y.; Malach, E.; Pražienková, V.; Maletínská, L.; Tempra, C.; Chamorro, V. C. et al. Sweet Taste of Heavy Water. Commun Biol 2021, 4, 1–10.
- (35) Ceriotti, M.; Bussi, G.; Parrinello, M. Langevin Equation with Colored Noise for Constant-Temperature Molecular Dynamics Simulations. Phys. Rev. Lett. 2009, 102, 020601.
- (36) Ceriotti, M.; Bussi, G.; Parrinello, M. Nuclear Quantum Effects in Solids Using a Colored-Noise Thermostat. *Phys. Rev. Lett.* **2009**, *103*, 030603.
- (37) Wang, H.; Sun, X.; Miller, W. H. Semiclassical Approximations for the Calculation of Thermal Rate Constants for Chemical Reactions in Complex Molecular Systems. J. Chem. Phys. 1998, 108, 9726–9736.
- (38) Sun, X.; Wang, H.; Miller, W. H. Semiclassical Theory of Electronically Nonadiabatic Dynamics: Results of a Linearized Approximation to the Initial Value Representation. J. Chem. Phys. 1998, 109, 7064–7074.
- (39) Liu, J.; Miller, W. H. A Simple Model for the Treatment of Imaginary Frequencies in Chemical Reaction Rates and Molecular Liquids. *J. Chem. Phys.* **2009**, *131*, 074113.
- (40) Feynman, R. P.; Hibbs, A. R.; Styer, D. F. Quantum Mechanics and Path Integrals; Courier Corporation, 2010.
- (41) Feynman, R. P. Statistical Mechanics; Addison-Wesley, 1972.
- (42) Berne, B. J.; Ciccotti, G.; Coker, D. F. Classical And Quantum Dynamics In Condensed Phase Simulations: Proceedings Of The International School Of Physics; World Scientific, 1998.
- (43) Tuckerman, M. E. Path integration via molecular dynamics. Quantum Simulations of Complex Many-Body Systems: From Theory to Algorithms 2002, 10, 269.

- (44) Herrero, C. P.; Ramírez, R. Path-Integral Simulation of Solids. *J. Phys.: Condens. Matter* **2014**, *26*, 233201.
- (45) Cao, J.; Voth, G. A. The Formulation of Quantum Statistical Mechanics Based on the Feynman Path Centroid Density. II. Dynamical Properties. J. Chem. Phys. 1994, 100, 5106–5117.
- (46) Jang, S.; Voth, G. A. A Derivation of Centroid Molecular Dynamics and Other Approximate Time Evolution Methods for Path Integral Centroid Variables. J. Chem. Phys. 1999, 111, 2371–2384.
- (47) Craig, I. R.; Manolopoulos, D. E. Quantum Statistics and Classical Mechanics: Real Time Correlation Functions from Ring Polymer Molecular Dynamics. J. Chem. Phys. 2004, 121, 3368–3373.
- (48) Witt, A.; Ivanov, S. D.; Shiga, M.; Forbert, H.; Marx, D. On the Applicability of Centroid and Ring Polymer Path Integral Molecular Dynamics for Vibrational Spectroscopy. J. Chem. Phys. 2009, 130, 194510.
- (49) Rossi, M.; Ceriotti, M.; Manolopoulos, D. E. How to Remove the Spurious Resonances from Ring Polymer Molecular Dynamics. *J. Chem. Phys.* **2014**, *140*, 234116.
- (50) Rossi, M.; Kapil, V.; Ceriotti, M. Fine Tuning Classical and Quantum Molecular Dynamics Using a Generalized Langevin Equation. *J. Chem. Phys.* **2018**, *148*, 102301.
- (51) Hele, T. J. H.; Willatt, M. J.; Muolo, A.; Althorpe, S. C. Boltzmann-Conserving Classical Dynamics in Quantum Time-Correlation Functions: "Matsubara Dynamics". *J. Chem. Phys.* **2015**, *142*, 134103.
- (52) Haggard, C.; Sadhasivam, V. G.; Trenins, G.; Althorpe, S. C. Testing the Quasicentroid Molecular Dynamics Method on Gas-Phase Ammonia. J. Chem. Phys. 2021, 155, 174120.

- (53) Fletcher, T.; Zhu, A.; Lawrence, J. E.; Manolopoulos, D. E. Fast Quasi-Centroid Molecular Dynamics. J. Chem. Phys. **2021**, 155, 231101.
- (54) Kapil, V.; VandeVondele, J.; Ceriotti, M. Accurate Molecular Dynamics and Nuclear Quantum Effects at Low Cost by Multiple Steps in Real and Imaginary Time: Using Density Functional Theory to Accelerate Wavefunction Methods. J. Chem. Phys. 2016, 144, 054111.
- (55) Marsalek, O.; Markland, T. E. Ab Initio Molecular Dynamics with Nuclear Quantum Effects at Classical Cost: Ring Polymer Contraction for Density Functional Theory. J. Chem. Phys. 2016, 144, 054112.
- (56) Uhl, F.; Marx, D.; Ceriotti, M. Accelerated Path Integral Methods for Atomistic Simulations at Ultra-Low Temperatures. *J. Chem. Phys.* **2016**, *145*, 054101.
- (57) Xue, Y.; Wang, J.-N.; Hu, W.; Zheng, J.; Li, Y.; Pan, X.; Mo, Y.; Shao, Y.; Wang, L.; Mei, Y. Affordable Ab Initio Path Integral for Thermodynamic Properties via Molecular Dynamics Simulations Using Semiempirical Reference Potential. J. Phys. Chem. A 2021, 125, 10677–10685.
- (58) Gui, X.; Fan, W.; Sun, J.; Li, Y. New Stable and Fast Ring-Polymer Molecular Dynamics for Calculating Bimolecular Rate Coefficients with an Example of OH + CH4.
 J. Chem. Theory Comput. 2022, 18, 5203–5212.
- (59) Ramírez, R.; López-Ciudad, T.; Noya, J. C. Feynman Effective Classical Potential in the Schrödinger Formulation. *Phys. Rev. Lett.* **1998**, *81*, 3303–3306.
- (60) Ramírez, R.; López-Ciudad, T. The Schrödinger Formulation of the Feynman Path Centroid Density. J. Chem. Phys. 1999, 111, 3339–3348.
- (61) Ramírez, R.; López-Ciudad, T. Phase-Space Formulation of Thermodynamic and Dynamical Properties of Quantum Particles. *Phys. Rev. Lett.* **1999**, *83*, 4456–4459.

- (62) Xu, X.; Chen, Z.; Yang, Y. Molecular Dynamics with Constrained Nuclear Electronic Orbital Density Functional Theory: Accurate Vibrational Spectra from Efficient Incorporation of Nuclear Quantum Effects. J. Am. Chem. Soc. 2022, 144, 4039–4046.
- (63) Xu, X.; Yang, Y. Full-Quantum Descriptions of Molecular Systems from Constrained Nuclear-Electronic Orbital Density Functional Theory. J. Chem. Phys. 2020, 153, 074106.
- (64) Xu, X.; Yang, Y. Constrained Nuclear-Electronic Orbital Density Functional Theory: Energy Surfaces with Nuclear Quantum Effects. J. Chem. Phys. 2020, 152, 084107.
- (65) Xu, X.; Yang, Y. Molecular Vibrational Frequencies from Analytic Hessian of Constrained Nuclear-Electronic Orbital Density Functional Theory. J. Chem. Phys. 2021, 154, 244110.
- (66) Karplus, M.; Porter, R. N.; Sharma, R. D. Dynamics of Reactive Collisions: The H+H2 Exchange Reaction. J. Chem. Phys. 1964, 40, 2033–2034.
- (67) Ceriotti, M.; More, J.; Manolopoulos, D. E. I-PI: A Python Interface for Ab Initio Path Integral Molecular Dynamics Simulations. Computer Physics Communications 2014, 185, 1019–1026.
- (68) Kubo, R. Statistical-Mechanical Theory of Irreversible Processes. I. General Theory and Simple Applications to Magnetic and Conduction Problems. J. Phys. Soc. Jpn. 1957, 12, 570–586.
- (69) Smith, K. K. G.; Poulsen, J. A.; Nyman, G.; Rossky, P. J. A New Class of Ensemble Conserving Algorithms for Approximate Quantum Dynamics: Theoretical Formulation and Model Problems. J. Chem. Phys. 2015, 142, 244112.
- (70) Guo, Y.; Thompson, D. L.; Sewell, T. D. Analysis of the Zero-point Energy Problem in Classical Trajectory Simulations. *J. Chem. Phys.* **1996**, *104*, 576–582.

- (71) Ben-Nun, M.; Levine, R. D. On the Zero Point Energy in Classical Trajectory Computations. J. Chem. Phys. 1996, 105, 8136–8141.
- (72) Einstein, A. Albert Einstein: Akademie-Vorträge; John Wiley & Sons, Ltd, 2005; pp 245–257.
- (73) Bose, Plancks Gesetz und Lichtquantenhypothese. Z. Physik 1924, 26, 178–181.
- (74) Unke, O. T.; Chmiela, S.; Sauceda, H. E.; Gastegger, M.; Poltavsky, I.; Schütt, K. T.; Tkatchenko, A.; Müller, K.-R. Machine Learning Force Fields. *Chem. Rev.* **2021**, *121*, 10142–10186.